High-Throughput Characterization of Single-Quantum-Dot Emission Spectra and Spectral Diffusion by Multiparticle Spectroscopy

Mark J. J. Mangnus, Jur W. de Wit, Sander J. W. Vonk, Jaco J. Geuchies, Wiebke Albrecht, Sara Bals, Arjan J. Houtepen, and Freddy T. Rabouw*

Cite This: https://doi.org/10.1021/acsphotonics.3c00420

Read Online

ACCESS | Metrics & More | Article Recommendations | Supporting Information

ABSTRACT: In recent years, quantum dots (QDs) have emerged as bright, color-tunable light sources for various applications such as light-emitting devices, lasing, and bioimaging. One important next step to advance their applicability is to reduce particle-to-particle variations of the emission properties as well as fluctuations of a single QD's emission spectrum, also known as spectral diffusion (SD). Characterizing SD is typically inefficient as it requires time-consuming measurements at the single-particle level. Here, however, we demonstrate multiparticle spectroscopy (MPS) as a high-throughput method to acquire statistically relevant information about both fluctuations at the single-particle level and variations at the level of a synthesis batch. In MPS, we simultaneously measure emission spectra of many (20−100)

QDs with a high time resolution. We obtain statistics on single-particle emission line broadening for a batch of traditional CdSe-based core−shell QDs and a batch of the less toxic InP-based core−shell QDs. The CdSe-based QDs show significantly narrower homogeneous line widths, less SD, and less inhomogeneous broadening than the InP-based QDs. The time scales of SD are longer in the InP-based QDs than in the CdSe-based QDs. Based on the distributions and correlations in single-particle properties, we discuss the possible origins of line-width broadening of the two types of QDs. Our experiments pave the way to large-scale, high-throughput characterization of single-QD emission properties and will ultimately contribute to facilitating rational design of future QD structures.

KEYWORDS: multiparticle spectroscopy, high-throughput single-particle spectroscopy, quantum dots, spectral diffusion, CdSe, InP
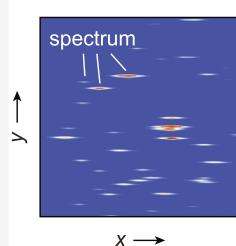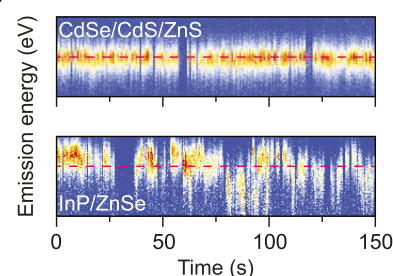
INTRODUCTION

Major advances in colloidal synthesis[1] have facilitated large-scale production of durable, color-tunable, and bright quantum dots (QDs) with applications in light-emitting diode (LED) devices,[2,3] lasing,[4] (bio)imaging,[5] and solar energy conversion.[6−9] In recent years, much effort has been directed at improving the quantum efficiency and/or color-purity of various types of QDs, including the traditional families of II−VI and III−V semiconductors, but also the more recently discovered perovskites[10] and nontoxic I−III−VI$_2$ QDs.[11] Narrow emission line widths and high photoluminescence quantum yields (PLQYs) are desired for many applications. Improving these key performance features requires uniform and well-defined emission properties for all QDs within a batch. However, eliminating property variations is challenging as the origins often remain obscured in ensemble measurements. Single-particle studies have revealed that the properties among single QDs can be very different, even when they originate from the same synthesis batch and are almost identical in terms of size, shape, and composition.[12−14] In fact, emission properties are not only different from one QD to

another but are also often unstable. This manifests as blinking and spectral diffusion (SD)—temporal fluctuations in the luminescence intensity and color.[15−24] Mechanisms of blinking and SD have been identified for different types of semiconductor QDs.[14,17−19,25,26] Knowledge of such undesired mechanisms has facilitated steps toward rational design of superior QDs—in particular CdSe-based core−(graded) shell heterostructures.[26−29] Despite these substantial developments, extending design rules to the more promising but less well-understood class of environmentally friendly III−V QDs remains challenging. The best results have been obtained with InP/ZnSe, InP/ZnS, or InP/ZnSe/ZnS core−shell-(−shell) structures,[30−37] but their mechanism of luminescence is still under discussion. In particular, while a type-I band
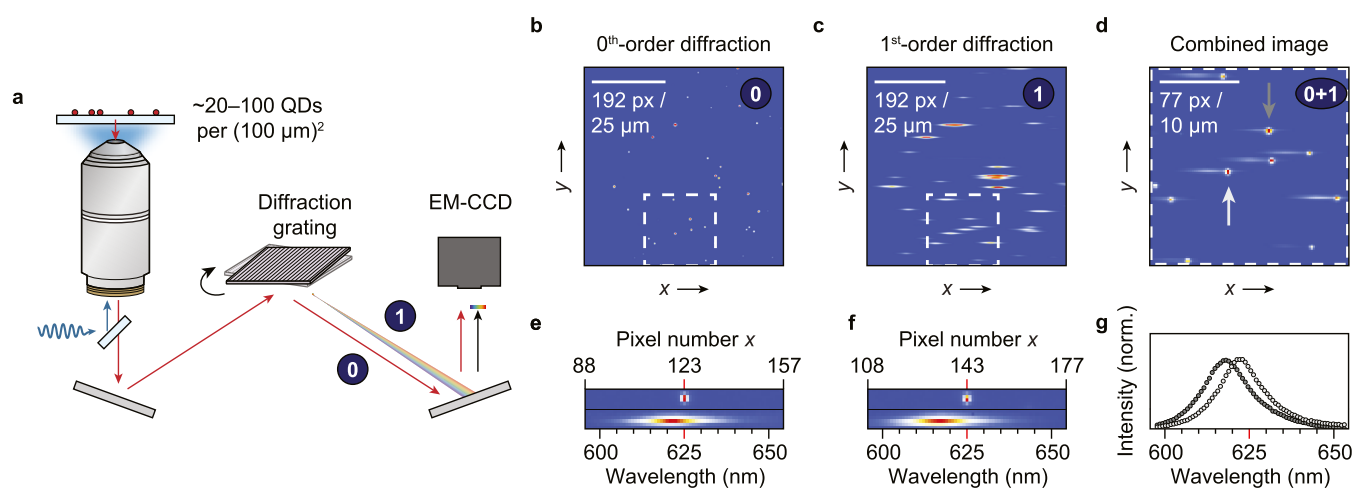
A

Figure 1. Multiparticle spectroscopy. (a) Luminescence from 20 to 100 QDs is collected simultaneously by a microscope objective. The image is directed to the entrance of a spectrometer (without the use of a slit) equipped with a diffraction grating. By positioning the grating at different angles, we project either the 0th-order reflection image (0) or the 1st-order diffraction image (1) onto a pixel-array camera. (b) Image of the 0th-order diffraction of a field of view containing several tens of CdSe/CdS/ZnS QDs. (c) The corresponding image of the dispersed 1st-order diffraction. The horizontally elongated emission spots contain spectral information. (d) Overlay of the 0th-order and 1st-order diffraction images. (e, f) Zoom-in views of the 0th-order and 1st-order diffraction images of the QDs highlighted in (d) (vertically offset for clarity). To obtain emission spectra, the wavelength axis is calibrated by fixing a center wavelength (625 nm in this experiment, approximately at the ensemble emission peak) at the pixel number x that corresponds to the center of the emission spot in the 0th-order diffraction image. (g) Resulting single-QD emission spectra of the two CdSe/CdS/ZnS QDs highlighted in (d).

alignment is often claimed based on the bulk band energies,[31,32,34,35] delocalization of the electron[38] or hole[36] into the ZnSe shell has also been proposed. Furthermore, defect-related trapping of charge carriers may strongly impact the nature of the exciton.[39−42] Experimental data with simultaneous single-particle detail and statistical relevance can help resolve such debates.

Here, we use multiparticle spectroscopy (MPS) as an unbiased high-throughput technique to study variations and fluctuations of the emission properties within batches of QDs. In MPS, we simultaneously excite many (20−100) QDs and spectrally disperse the photoluminescence from their diffraction-limited emission spots before focusing the image onto a pixel-array electron-multiplying CCD (EM-CCD) detector. Operating the EM-CCD at a frame rate of 10 Hz, we collect statistically relevant information about temporal fluctuations of single-particle emission spectra, as well as about particle-to-particle variations that occur within the batch. Compared to traditional single-particle spectroscopy, MPS facilitates a characterization speed that is at least 10 times faster and is unaffected by the problem of a user-selection bias.[43−46] We characterize the emission from a batch of CdSe-based and a batch of InP-based core−shell QDs (N = 491 for CdSe/CdS/ZnS and N = 154 for InP/ZnSe). The batch of InP/ZnSe QDs has more heterogeneous emission properties than the CdSe/CdSe/ZnS QDs and shows more SD. The time scales associated with SD in InP/ZnSe are longer than in CdSe/CdS/ZnS QDs. We ascribe the variations and fluctuations of single-QD properties to variations in size, shape, and materials properties and to the quantum-confined Stark effect (QCSE).[19,25,47] Interestingly, the strong SD observed in InP/ZnSe QDs can be explained both in the framework of a delocalized exciton and an exciton with a trapped charge carrier. The introduction of MPS in the field of colloidal QDs is an important step as it facilitates unbiased high-throughput characterization of single-particle emission properties that may greatly aid the development of future generations of QDs.

RESULTS AND DISCUSSION

Multiparticle Spectroscopy of Semiconductor Quantum Dots. The most common method to obtain emission spectra from individual QDs is time-consuming, making the acquisition of statistically relevant data difficult. Particles are typically measured one by one, guiding the emission of a QD through the narrow entrance slit of a spectrometer. The spectrometer contains a dispersing element such as a grating or a prism that disperses the light before it is projected onto a pixel-array camera. Calibration of the emission spectrum is relatively straightforward: all luminescence detected on the camera originates from a sharply defined position, and the light diffraction by the dispersing element is known. Measuring spectra of multiple QDs in this way usually involves scanning over the sample area, although it is possible to use a densely covered substrate and measure several QDs at different vertical positions within the slit simultaneously.[48]

Rather than measuring the photoluminescence of selected QDs one by one, we use MPS to measure emission spectra of typically 20−100 QDs simultaneously. The method is inspired by a recent study of QD blinking at the multiparticle level[49] and slitless strategies that have previously been applied in the fields of bioimaging and astrophysics.[50−52] In MPS (Figure 1a), QDs are sparsely distributed on a glass substrate and excited by wide-field illumination. Without the use of an entrance slit, the emission from these QDs is directed to our spectrometer that is equipped with a reflective diffraction grating. Depending on the orientation of the diffraction grating in the spectrometer, either the 0th-order (i.e., the specular) reflection or the 1st-order diffraction is projected onto our pixel-array EM-CCD camera. The 0th-order reflection is just the real-space image of the field of view containing information about the position of the individual emitters (see Figure 1b; an example of a measurement on CdSe/CdS/ZnS core−shell QDs). In the 1st-order diffraction (Figure 1c), light of different colors is dispersed at different angles, with blue light diffracted
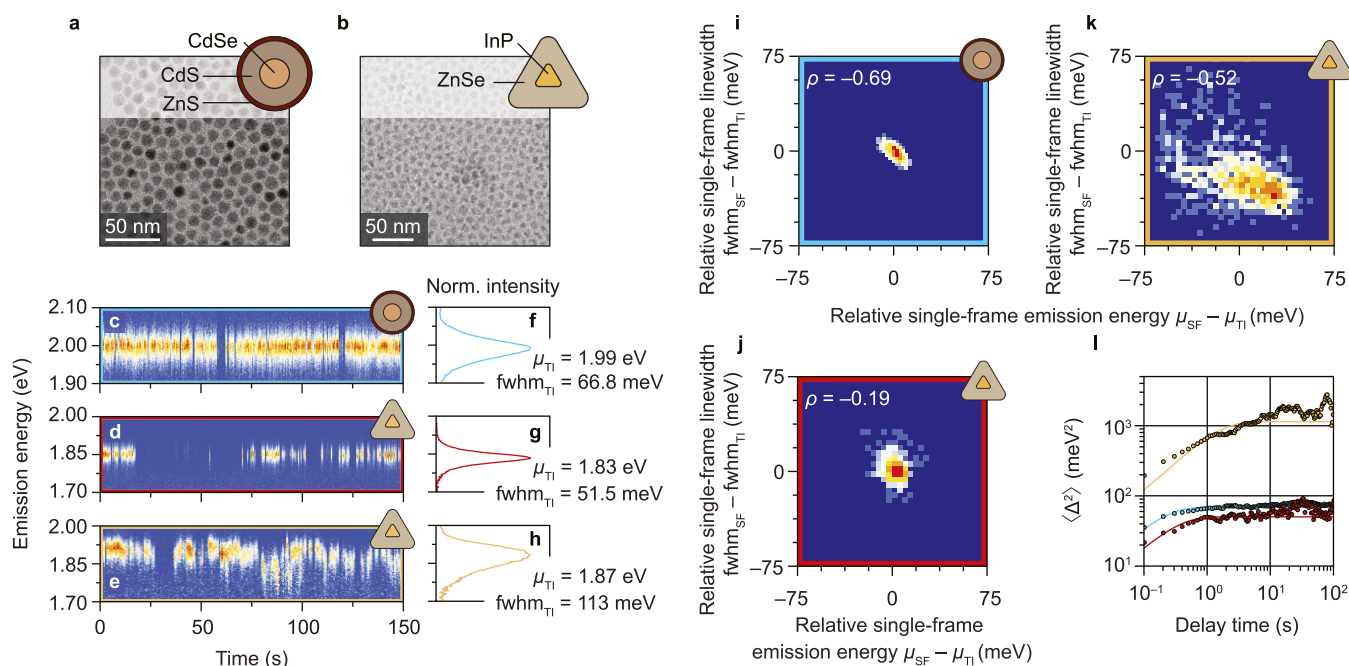
Figure 2. Spectral diffusion of single QDs. (a, b) Transmission electron microscopy images of the CdSe/CdSe/ZnS core−shell QDs and InP/ZnSe QDs. Geometries of the core−shell(−shell) QDs are schematically shown in the insets. (c) Time trace of the emission spectra of a representative CdSe/CdS/ZnS QD with a 100 ms time resolution. (d, e) Same as (c), but for two InP/ZnSe QD that exhibit weak and strong spectral diffusion. (f−h) Time-integrated emission spectra corresponding to the time traces in (c)−(e). (i−k) Correlation between the single-frame (100 ms) emission energy and line width, μ_{SF} and $fwhm_{SF}$. The correlations are shown as two-dimensional (2D) histograms of μ_{SF} and $fwhm_{SF}$, relative to the time-integrated peak energy and line width, for the QDs in (c)−(h) (same colors). Note that the histograms are centered at values (just) below (0, 0) as the single-frame line width is narrower than the time-integrated line width. (l) Mean square energy difference, $\langle\Delta^2\rangle$, of the emission energy as a function of the delay time between recorded frames. Colors correspond to the colors in (c)−(h). Solid lines are fits to eq 1.

at smaller angles and red light at wider angles. The image of the 1st-order diffraction thus contains the spatial information in one dimension (vertical), while the other dimension (horizontal) is a convolution of spatial and spectral information (see Figure 1c). Overlaying the 0th-order and 1st-order diffraction images (Figure 1d), we see clearly that the emission from each individual QD is dispersed horizontally around its original position. We used a background-subtraction procedure to obtain the clean images in Figure 1b−f, as explained in the Supporting Information, Section S2. The horizontal positions of the diffraction-limited emission spots in the 0th-order diffraction image form the basis for wavelength calibration of the numerous emission spectra in Figure 1c: the horizontal pixel number of the emission spot coincides with a center wavelength around which the light is dispersed (see Figure 1e,f). The wavelength of pixel position x_1 in the 1st-order diffraction image is calibrated as $\lambda(x_1) = \lambda_{cent} + d\lambda(x_1 - x_0^*)$, with λ_{cent} the grating's center wavelength, which depends on the grating orientation, x_0^* the pixel position of the QD in the 0th-order diffraction image, and $d\lambda = c_{x_1-x_0^*} d\lambda_0$. $c_{x_1-x_0^*}$ is a correction factor that accounts for a small dependence of $d\lambda$ on x (ranges from 1.01 to 0.99 for the leftmost and rightmost pixels). Using this calibration, we can reconstruct the emission spectra of many individual QDs simultaneously (Figure 1g). We verified that this calibration procedure of our MPS images returns a QD emission spectrum correctly, independently of the horizontal position of the QD on the sample (Supporting Information, Section S3), and confirmed that the sample does not drift on the time scale of our measurements (Supporting Information, Section S5).

Using MPS, we can measure the emission spectra of many single QDs with high time resolutions down to ca. 20−100 ms (depending on the signal-to-noise requirements), resolving the behavior of both blinking and SD. As we can simultaneously characterize 20−100 QDs, it is possible to measure hundreds of QDs within an hour—more than 10 times faster than single-particle spectroscopy, and without user-selection bias. An even better level of statistical information about single-QD line widths and SD, and with better time resolution down to the ns range, can be obtained using solution-phase photon-correlation Fourier spectroscopy (sPCFS).[43,53,54] However, sPCFS does not capture SD because each individual QDs is probed for no longer than a couple of milliseconds as they move through the detection volume.[54] Furthermore, it provides information only about average single-particle line widths and relative emission energies. sPCFS thus does not offer a complete picture of emission variations and fluctuations. Our strategy of MPS fills the gap of high-throughput characterization of absolute emission energies, variations in single-particle properties, and SD (at 10^{-2}–10^3 s time scales) with a good level of statistics. According to previous sPCFS measurements,[54] this range of accessible time scales is exactly the interesting range in which SD occurs.

In this manuscript, we first demonstrate examples of single-particle emission properties that can be extracted from high-throughput MPS measurements, before characterizing variations among particles within a batch. We finish by identifying correlations in the particle-to-particle variations and we discuss the different behaviors observed for CdSe/CdS/ZnS and InP/ZnSe QDs.
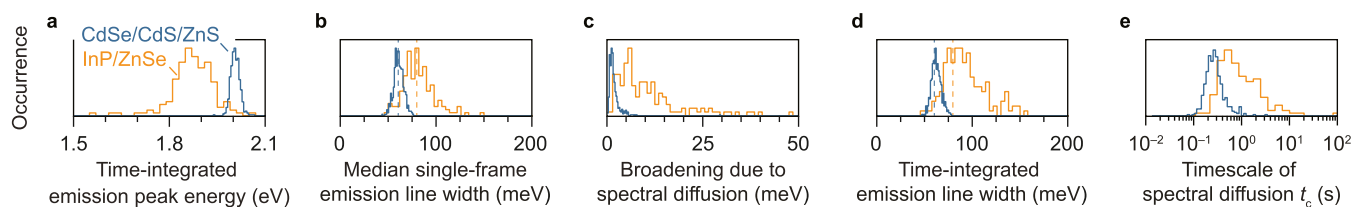
Figure 3. Variations in single-particle emission properties within batches of QDs. (a) Distribution of the time-integrated emission energy, (b) single-frame emission line width, and (c) spectral diffusion-induced broadening. (d) As a result of spectral diffusion, the time-integrated emission line width is broadened with respect to the single-frame line width. (e) Histograms of the relevant time scales associated with SD. Results are shown for 491 CdSe/CdS/ZnS and 154 InP/ZnSe QDs (blue and yellow histograms, respectively).

Spectral Diffusion of Single CdSe/CdS/ZnS and InP/ZnSe Core−Shell Quantum Dots. MPS at high frame rates reveals SD, i.e., fluctuations of the emission spectrum, of all QDs in the field of view simultaneously. To optimize fluorescence signal while maintaining a high time resolution, we measured SD at a frame rate of 10 Hz for two different types of QDs: a batch of CdSe/CdS/ZnS (N = 491) and a batch of InP/ZnSe (N = 154) core−shell QDs. The CdSe/CdS/ZnS QDs are the same batch as measured in ref 55. The QDs are spherical, with a core diameter of 3.7 nm, and the shell consists of 8 monolayers of CdS and 2 monolayers of ZnS so that the total QD diameter is 9.2 ± 0.8 nm (mean ± standard deviation).[55] The InP/ZnSe QDs are truncated tetrahedrons[56] with a core size of 3.2 nm and an edge length of 10.5 ± 1.2 nm (Figure 2a,b). The CdSe/CdS/ZnS QDs show minor SD. A representative time trace of the emission spectrum is shown in Figure 2c. Upon close inspection, small jumps (<5 meV) of the emission peak are apparent. Two different types of behavior, observed in two different InP/ZnSe QDs from the same synthesis batch, are shown in the time traces in Figure 2d,e. The first InP/ZnSe QD (Figure 2d) exhibits SD similar to that of our CdSe/CdS/ZnS QDs, featuring only small spectral jumps. The second QD (Figure 2e), on the other hand, shows spectral jumps as large as 100 meV, as well as more gradual shifts. For every 100 ms spectral frame, we fitted an empirical Gaussian function to estimate the single-frame emission peak energy μ_{SF} and line width fwhm$_{SF}$. The emission peak energy μ_{SF} exhibits fluctuations because of SD, which increases the line width of the time-integrated emission spectra (Figure 2f–h). In the following analysis of emission energy and line width, we used an intensity threshold to reject frames during which the QD blinked off (Supporting Information, Section S4).

More information about SD is encoded in the correlation between the emission energy and line width that a single QD features over the recorded frames. We describe the correlation in terms of the Pearson correlation coefficient $\rho_{\mu,fwhm}$: the covariance of μ_{SF} and fwhm$_{SF}$ normalized to the product of their respective standard deviations. Possible values range from −1 (perfect negative correlation) to +1 (perfect positive correlation). Figure 2i shows a 2D histogram of the single-frame emission energies and line widths for the CdSe/CdS/ZnS that was previously highlighted in Figure 2c. Higher emission energies μ_{SF} are correlated with narrower line widths fwhm$_{SF}$, with a $\rho_{\mu,fwhm}$ of −0.69. The two previously selected InP/ZnSe QDs exhibit two different types of behavior, with the first showing a weak negative correlation between μ_{SF} and fwhm$_{SF}$ and the second showing a more pronounced correlation ($\rho_{\mu,fwhm}$ of −0.19 and −0.52, respectively). 2D histograms are shown in Figure 2 j–k. We will further discuss the observed correlations at a later point.

Based on the emission time traces (Figure 2c−e), SD in the CdSe/CdS/ZnS and InP/ZnSe QDs appears to occur at time scales of seconds, although it is not possible to identify SD at sub-100-ms time scales because of the time resolution. To quantify the relevant time scale at which SD occurs, we calculate the mean square energy difference between emission peaks, $\langle \Delta^2 \rangle = \langle [\mu_{SF}(t) - \mu_{SF}(t + \tau)]^2 \rangle_t$, as a function of delay time τ between frames (Figure 2l). The emission energies of a QD are correlated at short delay times, as indicated by the small $\langle \Delta^2 \rangle$. For longer delay times, $\langle \Delta^2 \rangle$ increases because of the fluctuations in emission energy, which we observed directly in Figure 2c−e. $\langle \Delta^2 \rangle$ reaches a plateau at delay times of several seconds, indicating that the spectrum wanders within finite bounds. The $\langle \Delta^2 \rangle$-curves of the CdSe/CdS/ZnS QD and the two selected InP/ZnSe QDs (Figure 2l) are qualitatively similar. However, the characteristic time scales at which SD takes place are different. We determine the characteristic time scale of SD, t_c, by fitting the model function

$$\langle \Delta^2 \rangle(\tau) = \Delta_\infty^2 (1 - e^{-\tau/t_c}) + 2\sigma^2 \tag{1}$$

to the experimental $\langle \Delta^2 \rangle$-curve, where Δ_∞^2 is the plateau value and $2\sigma^2$ is a constant offset accounting for the fit error on the single-frame emission peak energy (Supporting Information, Section S5). The exponential term is exactly the expected time dependence of $\langle \Delta^2 \rangle$ for a single charge diffusing randomly on the surface of a spherical QD with a polarized exciton (Supporting Information, Section S6) but may also be the result of more complex charge diffusion and a polarizable exciton. This model function provides a reasonable estimate for the magnitude and time scale of SD, but is not an equally perfect match to all experimental $\langle \Delta^2 \rangle$-curves. The selected CdSe/CdS/ZnS QD of Figure 2c has $\Delta_\infty^2 = 6.5 \times 10^2$ meV^2 and $t_c = 0.16$ s (blue solid line in Figure 2l). The two InP/ZnSe QDs yield fit parameters $\Delta_\infty^2 = 4.7 \times 10^1$ meV^2 and $t_c = 0.26$ s and $\Delta_\infty^2 = 1.1 \times 10^3$ meV^2 and $t_c = 1.2$ s, respectively (Figure 2l). Based on the values for t_c, we can conclude that for all QDs, SD probes the full range of possible emission energies μ_{SF} (distributions in Figure 2f−h) within a time scale of a few seconds. As indicated by the higher plateau value of the orange $\langle \Delta^2 \rangle$-curve in Figure 2l, the range of energies over which μ_{SF} fluctuates is much larger for this InP/ZnSe QD compared to the other QDs. This is consistent with the time traces in Figure 2c−e.

Interparticle Variations within Batches of QDs. Our method of MPS can statistically map out single-particle fluctuations (Figure 2) on the one hand, and interparticle variations on the other hand. Together, they determine the emission properties of a batch of QDs. In Figure 3a, we show the inhomogeneous broadening of our batches of CdSe/CdS/ZnS and InP/ZnSe QDs, i.e., the distributions of time-
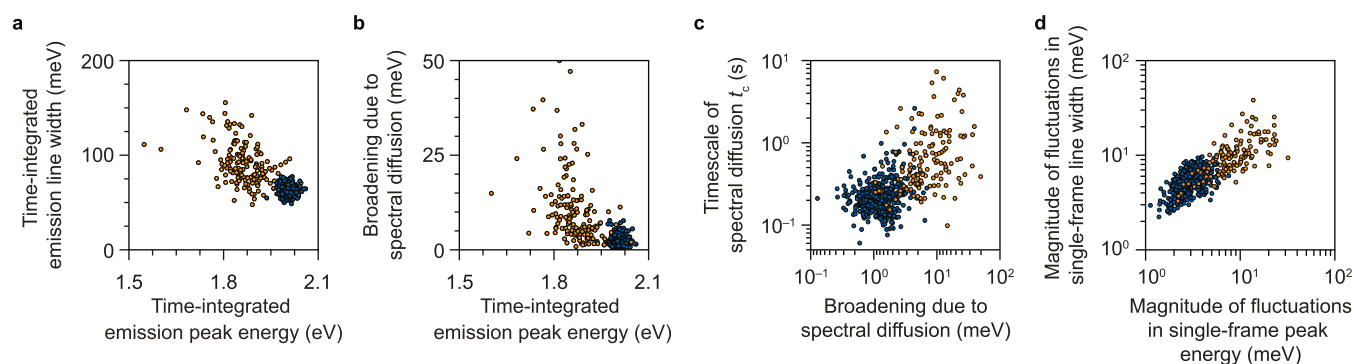
Figure 4. Correlations in single-particle emission properties. Each data point in (a)−(d) represents an individual QD. Results for CdSe/CdS/ZnS (blue) and InP/ZnSe (yellow) are shown in the same plots. (a) Correlation between the emission peak energy and line width. (b) Relationship between the SD-induced line broadening and the emission energy of the QDs. (c) Correlation between the time scale of SD and broadening due to SD. (d) Magnitude of single-particle fluctuations in emission peak energy μ_{SF} and line width fwhm$_{SF}$.

integrated emission maxima (491 and 154 single-particle measurements, respectively). It is immediately evident that the batch of CdSe-based core−shell QDs has a more well-defined emission energy, while the batch of InP/ZnSe QDs shows wider variations. The CdSe/CdS/ZnS QDs emit at 2.004 ± 0.014 eV and the InP/ZnSe QDs at 1.86 ± 0.07 eV. The single-frame emission line width fwhm$_{SF}$ is a measure for the homogeneous emission line width (Figure 3b), only affected by SD-induced broadening on sub-100-ms time scales.[54,57] For CdSe/CdS/ZnS, this single-frame line width is narrow for all particles: 61 ± 5 meV. The batch of InP/ZnSe, instead, features a broader average line width and a much wider spread: 80 ± 16 meV.

Fluctuations of the emission spectrum are observed in both types of QDs, as previously highlighted in Figure 2. For the batch of CdSe/CdS/ZnS QDs, a large majority of 67.3% of QDs exhibit a clear negative correlation between emission energy and line width ($-1.00 < \rho_{\mu,fwhm} < -0.25$). In other words, most single-QD spectra broaden when they shift toward the red, similar to Figure 2i. For the remaining QDs, a clear negative correlation may be obscured by the fit uncertainty which is large compared to the SD-induced spread of emission properties (Supporting Information, Section S7). Most InP/ZnSe QDs (76.1%) also exhibit spectral diffusion where the emission energy and line width are negatively correlated, similar to Figure 2k. The other QDs show no clear correlation, similar to Figure 2j. Hence, the SD in CdSe/CdS/ZnS and InP/ZnSe QDs are alike in terms of the predominantly negative correlation between μ_{SF} and fwhm$_{SF}$. Realize that $\rho_{\mu,fwhm}$ quantifies the degree of correlation but does not carry information about the ranges of μ_{SF} and fwhm$_{SF}$ over which the single-QD spectrum fluctuates.

We define the SD-induced broadening of the emission spectrum as the difference between the time-integrated and the median single-frame line width. Histograms of this SD-induced broadening and the resulting time-integrated emission line widths are shown in Figure 3c,d. The CdSe-based QDs show minor SD, with a broadening of only 1.5 ± 0.8 meV and thus the time-integrated line width (62 ± 5 meV) is almost identical to the single-frame line width (61 ± 5 meV). The batch of InP-based QDs, on the other hand, features QDs with strong SD. The SD-induced broadening of 10 ± 7 meV (mean ± standard deviation) is a substantial contribution to the time-integrated emission spectra that have a line width of 92 ± 25 meV, compared to 80 ± 16 meV for the single-frame line width. We

note that our batch of InP/ZnSe QDs is highly heterogeneous: while some QDs are strongly affected by SD and feature emission line widths as broad as 120−150 meV, others are only mildly affected by SD and have emission spectra as narrow as 50−60 meV—comparable or even superior to the Cd-based QDs. Figure 3e shows the distribution of relevant time scales associated with SD in the two batches of CdSe/CdS/ZnS and InP/ZnSe. The characteristic time scale of SD t_c (eq 1) in the CdSe/CdS/ZnS QDs is rather uniform, with values of 0.22 ± 0.08 s (mean ± standard deviation). In our InP/ZnSe t_c is 0.9 ± 0.9 s, which is four times longer on average and more widely distributed.

Based on the distributions of emission properties we can conclude that the batch of CdSe/CdS/ZnS is a superior batch of QDs, with little inhomogeneous broadening (Figure 3a), and a narrow (Figure 3b) and stable (Figure 3c) single-particle emission line width. Instead, the batch of InP/ZnSe QDs is highly diverse, containing some high-quality QDs with narrow emission line widths (Figure 3d), but also containing a large fraction of QDs that is severely affected by SD (Figure 3c). We speculate that the large variations in emission properties among particles in our batch of InP/ZnSe QDs may be a consequence of variations in size, geometry, composition,[38] and defects.[39−42] This discussion will be resumed later. At this point, we emphasize that the heterogeneity of emission properties observed in this batch highlights the unique capabilities of MPS to characterize particle-to-particle variations of the emission properties with strong statistics and without a user-selection bias.

Having characterized the variations between particles within the two batches of QDs, we will now explore possible correlations in the emission properties. We did not observe clear trends related to the brightness of the QDs, which suggests that SD cannot be linked to large variations in the PLQY, and hence will not discuss intensity-based correlations in the following discussion. Figure 4a shows the relation between the emission peak energy and the broadening due to SD. Interparticle variations are uncorrelated for CdSe/CdS/ZnS QDs. For InP/ZnSe QDs, instead, lower emission energies appear to be associated with broader line widths. Figure 4b shows the possible correlation between the emission peak energy and the broadening due to SD. There is no clear correlation for the CdSe/CdS/ZnS QDs, while for the InP/ZnSe QDs stronger SD-induced broadening appears to be correlated with lower emission energies. Figure 4c shows a

positive correlation between the time scale of SD t_c and the SD-induced emission line broadening.

Figure 4d highlights the magnitude of the fluctuations in emission energies and line widths due to SD. Large fluctuations of μ_{SF} are in general associated with concomitant large fluctuations in fwhm$_{SF}$. Both μ_{SF} and fwhm$_{SF}$ fluctuate by up to 30 meV for InP/ZnSe versus approximately 2−6 meV for CdSe/CdS/ZnS. The magnitude of the fluctuations is unrelated to the correlation coefficient (Supporting Information, Figure S7) but is, on average, very different between the two types of QDs.

DISCUSSION

We can explain the SD of both batches of QDs (Figures 3 and 4) in terms of the commonly invoked QCSE.[14,19,25,47] The QCSE is the energy shift of the exciton state due to polarization by an electric field. A fluctuating electric field, and hence fluctuating exciton energy, is thought to originate from the random movement of mobile charges.[58] These charges may be charged ligands hopping from site to site, or charge carriers hopping between trap states on the surface or inside the QD. If such hopping occurs on time scales of milliseconds to seconds, it manifests as SD. The quantitative effect, i.e., the magnitude of emission shift, depends on the charge distribution in the excited state of the QDs and on the position and charge of species on the QD surface. In the following discussion, we shall take into account the nature of the excited states in our CdSe/CdS/ZnS and InP/ZnSe QDs to explain the differences in their interparticle variations and fluctuations.

Mobile charges at the QD surface cause an electric field across the QD and polarize the exciton wavefunction, which not only lowers the emission energy (i.e., QCSE) but also broadens the spectrum because of enhanced coupling of the polarized exciton to optical phonons.[19,25,47] This twofold effect of wavefunction polarization causes the negative correlation between emission energy and line width, which has been reported before for CdSe-based core−shell structures.[19,59] Our experimental results reproduce this clear negative correlation for the majority of the CdSe/CdS/ZnS (Figure 2i) and InP/ZnSe QDs (Figure 2k). The correlation is less clear for a subset of the QDs but, as discussed above, this may be a result of fit uncertainties that are large compared to the observed SD-induced spread of μ_{SF} and fwhm$_{SF}$ (Supporting Information, Section S7).

The CdSe/CdSe/ZnS QDs show a minor SD-induced broadening of 1.5 ± 0.8 meV (Figure 3c), seemingly uncorrelated to the emission energy (Figure 4b). This corresponds with fluctuations of the exciton energy of 3.2 ± 1.0 meV (Figure 4d; convolution with the single-frame line width produces the 1.5 ± 0.8 meV broadening; see Supporting Information, Figure S8). The model of the QCSE predicts that the exciton energy red-shifts by an amount

$$\Delta E = \mathbf{p} \cdot \mathbf{F} - \frac{1}{2}\alpha F^2 \tag{2}$$

because of an instantaneous electric field $\mathbf{F}$ due to mobile surface charges.[14,25,47] Here, the first term describes the interaction of the external electric field with a static dipole moment of the excited state $\mathbf{p}$, which may be absent ($p = 0$) but can arise due to asymmetric (de)localization of the charge carriers. The second term is the effect of the polarizability α of the exciton wavefunction. High-resolution scanning trans-

mission electron microscopy and energy dispersive X-ray (EDX) mapping show that our CdSe/CdS/ZnS QDs may have slight off-center positions of the CdSe core (Supporting Information, Section S8). As the electron delocalizes over the CdS shell while the hole is confined to the core, an asymmetric shell could produce a small dipole moment $\mathbf{p}$. However, previous experiments with intentional external electric fields have shown that the quadratic term in eq 2 is the dominant contribution to the QCSE in spherical CdSe-based nanocrystals.[25,47]

The magnitude of the energy fluctuations depends on the maximum electric field that the exciton may experience due to the fluctuating charges on the QD surface. As a back-of-the-envelope calculation, we consider the maximum electric field F_{max} in the center of a spherical QD of radius R due to two elementary charges at opposite side of the surface[14,25,47]

$$F_{max} \approx \frac{e}{2\pi\varepsilon\varepsilon_0 R^2} \tag{3}$$

where e is the elementary charge, ε_0 is the vacuum permittivity, and ε is the relative permittivity of the QD material. The QCSE is consistent with the estimated polarizability of the exciton in our CdSe/CdS/ZnS QDs, which, to first order, is the sum of electron and hole contributions:[14,25]

$$\alpha = \alpha_e + \alpha_h = 0.036\frac{e^2}{\hbar^2}(m_e R_e^4 + m_h R_h^4) \tag{4}$$

with $m_{e,h}$ the effective masses of the electron and hole, and $R_{e,h}$ the radii of the volumes in which the electron and hole are delocalized. The contributions of the electron and hole to the exciton polarizability are $\alpha_e/4\pi\varepsilon_0 = 2 \times 10^4$ Å^3 and $\alpha_h/4\pi\varepsilon_0 = 8 \times 10^3$ Å^3, as estimated assuming an electron with $m_e = 0.11\ m_0$ delocalized into the CdS shell and a core-confined hole with $m_h = 1.14\ m_0$.[60,61] Fluctuating electric fields on the order of 20 MV m^{-1} (eq 3) would hence explain emission energy fluctuations of 3.2 ± 1.0 meV. The low polarizability and a small off-center position of the CdSe core can thus explain the minor impact of SD on our CdSe/CdS/ZnS QDs (Figure 5a,b). As a side note: as α scales with the fourth power of R_e and R_h (eq 4) and F scales with the inverse second power of the QD size, the quadratic energy term of the QCSE ($\frac{1}{2}\alpha F^2$ in eq 2) depends hardly on QD size.

The clear negative correlation between fluctuations in μ_{SF} and fwhm$_{SF}$, which we (Figure 2i) and others[19,59] have observed in many single CdSe-based QDs, is not obvious for interparticle variations within the batch of CdSe/CdS/ZnS ($\rho_{\mu,fwhm}$ of −0.08; Figure 4a). We conclude that fluctuations at the single-particle level and interparticle variations must have different underlying causes. Although the correlated fluctuations in emission energy and line width are consistent with the QCSE, the uncorrelated variations at the ensemble level are likely simply due to (slight) variations in size and/or shape/geometry of the QDs (Supporting Information, Section S8), while differences in wavefunction polarization play no significant role.

The fluctuations of InP/ZnSe QDs are also consistent with the QCSE. However, the emission properties of our InP/ZnSe QDs are clearly more broadly distributed (Figure 3a) and fluctuate more (Figure 3b,c) than those of the CdSe/CdS/ZnS QDs. This wider inhomogeneous broadening of InP-based confirms previous studies, which found similar trends.[37,43] To understand why the InP/ZnSe QDs are so different
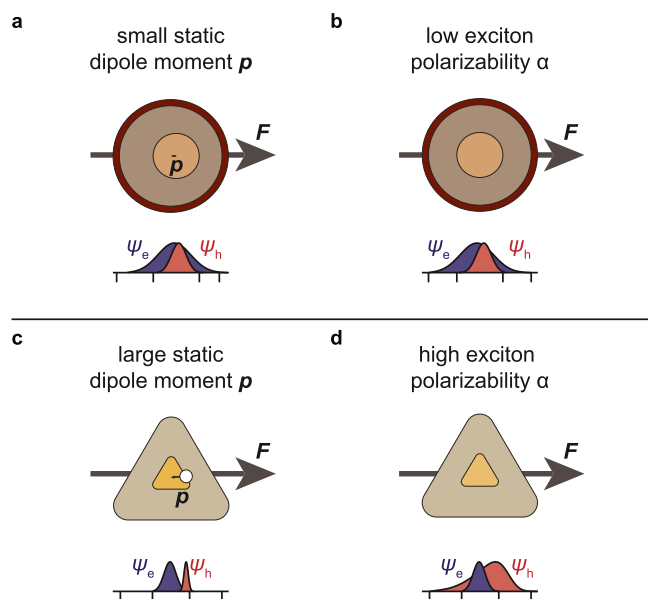
Figure 5. Linear and quadratic contributions to spectral diffusion. (a) CdSe/CdS/ZnS core–shell–shell QDs are nominally spherically symmetric but a small offset of the core may result in a small intrinsic dipole moment of the excited state p. (b) Exciton polarizability in CdSe/CdS/ZnS QD is low because the electron effective mass is low and the hole's delocalization volume is small. (c) The proposal of hole localization at defect sites in InP-based QDs[39,41,42] comes with a static dipole moment p in the excited state. Depending on the position of this defect site, the interaction with external electric fields may be strong. (d) The proposal of the hole delocalization into the shell implies a large polarizability of the exciton, as the effective mass of the hole is large. This would make the exciton energy strongly dependent on fluctuating electric fields.

quantitatively, we consider two types of proposals for the nature of the excited state in InP/ZnSe.

Shallow electron or hole traps in InP-based QDs have been proposed, such as Zn on an In site in the core or In on a Zn shell in the shell,[39−42] from which radiative recombination could occur. Carrier localization should be associated with large lattice reorganizations and thus a red shift and line broadening of the emission.[14,39,41,42] The proposal of carrier localization also implies reduced electron−hole wavefunction overlap, which is consistent with previous observations that exciton lifetimes are longer at the low-energy side of the emission spectrum.[62,63] The degree of carrier localization may vary depending on the interdiffusion of core and shell materials, which could cause the variations between QDs: deeper localization causes a stronger red shift and more broadening. Indeed, we observe that QDs emitting at lower energies typically have broader time-integrated (Figure 4a; correlation coefficient $\rho_{\mu,fwhm} = -0.48$) as well as single-frame (Supporting Information, Section S9) line widths. Localization of a charge carrier at defect sites can also result in a significant static dipole moment $\mathbf{p}$ in the excited state. This would interact strongly with fluctuating external electric fields through the linear term in eq 2,[25] as has previously been observed for CuInS$_2$ QDs.[13,14] For example, if the hole is trapped 1 nm off-center while the electron occupies the entire InP core, this creates a dipole moment with magnitude $p = 1.6 \times 10^{-28}$ Cm. In the presence of an external field of 20 MV m^{-1} of an InP/ZnSe QD, the emission energy may change by as much as 20 meV. This is consistent with the observed fluctuations of the

emission maximum of 11 ± 7 meV due to SD (Figure 4d and Supporting Information, Figure S8).

An opposite picture of the excited state of InP/ZnSe QDs has also been proposed, in which the hole delocalizes into the ZnSe shell and the electron remains core-confined.[36] While InP/ZnSe would be a type-I QD according to the bulk band alignments, a charge disbalance at the core−shell interface could change the band offsets and cause hole delocalization.[38] Full delocalization of the hole would increase its polarizability α_h 100-fold according to eq 2, going from $R_h = 1.5$ nm for a core-localized hole to $R_h = 4$ nm for a delocalized hole. As the hole in InP is relatively heavy ($m_h = 0.6\ m_0$; ref 34), the overall exciton polarizability of our InP/ZnSe QDs would be as high as $\alpha/4\pi\varepsilon_0 = 3 \times 10^5$ Å^3. The 10-fold higher exciton polarizability in InP-base QDs compared to CdSe-based QDs may thus be responsible for the strong SD observed in (some of) the InP/ZnSe QDs. The interparticle variations in emission energy and line width could be due to differences in the charge disbalance at the core−shell interface, which would cause differences in delocalization and hence differences in polarizability. In this picture, correlations between emission energy and line broadening emission (Figure 4a,b) could also be due to the degree of (de)localization.

The two possible options for the nature of the excited state in CdSe/CdS/ZnS and InP/ZnSe are illustrated in Figure 5. Ironically, both a localized and a delocalized hole can explain the strong SD that we observe for our InP/ZnSe QDs. In the case of a localized hole, the static dipole moment $\mathbf{p}$ of the excited state increases the influence of the QCSE through the linear term in eq 2. In the case of a delocalized hole, the exciton polarizability α is high and the influence of the QCSE is strong through the quadratic term in eq 2. Interparticle variations in the degree of (de)localization may well explain the strong inhomogeneous broadening that we and others[37,39,43,64] have observed for InP/ZnSe QDs.

The different characteristic time scales of SD, as observed in Figure 4c may be explained in terms of the different geometries of the CdSe/CdS/ZnS and InP/ZnSe QDs. Specifically, the spherical geometry of the Cd-based core−shell−shell QDs implies that the energy shift of the exciton depends only on the magnitude of the fluctuating charge disbalance on the QD surface, irrespectively of where this charge disbalance occurs. The InP/ZnSe truncated tetrahedra lack this spherical symmetry so different possible locations of mobile charge on the surface are inequivalent. For example, the exciton would be affected less by a surface charge disbalance at the apices of the tetrahedron than by one at the sides. The longer time scale of SD in InP/ZnSe may be a consequence of this lower symmetry: mobile surface charges need to move over a larger area of inequivalent positions on the QD surface before all possible emission energies are sampled. An alternative explanation may be that the nature of the mobile charges is different. Their mobilities may depend on the surface chemistry of the QD.

Further experiments are required to get a complete picture of SD and its underlying chemophysical dynamics. Regarding our CdSe/CdS/ZnS and InP/ZnSe QDs, characterizing SD while externally controlling the static electric fields across the QDs[25,47] may distinguish between contributions of a static dipole moment (producing a linear field dependence; eq 2) and/or strong polarizability of the exciton wavefunction (quadratic field dependence; eq 2). Information from single-particle lifetimes and excitation spectra may further help settle

this debate. The relevant time scales associated with SD—on the order of seconds—may be related to binding and dissociation of ligands on the surface. Such processes typically have an activation energy that could be extracted from temperature-dependent experiments or a systematic study with different types of capping ligands. To design future QDs with reduced SD, anchoring ligands in a rigid inorganic shell[65] could be a promising strategy.

■ CONCLUSIONS

In summary, we have introduced MPS as a high-throughput method to measure individual emission spectra of 20−100 single emitters simultaneously at relevant time scales ranging from tens of milliseconds to several minutes. MPS provides statistically relevant information about variations and fluctuations in absolute emission spectra. The results are not affected by an undesired user-selection bias that is inherent to single-particle spectroscopy. Using MPS, we characterized the variations of the emission properties in a batch of CdSe/CdS/ZnS and InP/ZnSe QDs. We find that the CdSe/CdS/ZnS QDs have a well-defined emission energy and a narrow line width (62 ± 5 meV). Our batch of InP/ZnSe is much more diverse, with a wide distribution of emission energies and featuring both wide and narrow line widths (92 ± 25 meV). Although the line width of our CdSe/CdS/ZnS QDs is hardly affected by SD (broadening of 1.5 ± 0.8 meV), SD can play a substantial role for InP/ZnSe QDs (10 ± 7 meV). For most QDs, SD exhibits a negatively correlated behavior between single-frame emission energy and line width, which we ascribe to the QCSE. Differences in homogeneous broadening and SD between the two types of QDs are likely related to differences in charge distribution/localization in the excited state or differences in crystallite symmetry. Our data and discussion may help in the further understanding of the excited states of InP-based QDs, which is not yet as mature as for CdSe-based QDs. Various variations and extensions of the MPS method are possible, such as cryogenic measurements on the simultaneous diffusion of dark and bright exciton, trion, and/or biexciton emission lines,[66] or polarization-resolved measurements to correlate emission properties with nanocrystal anisotropy.[67] MPS could further allow for statistically significant studies of the influence of external parameters on single-QD emission, such as ligand coverage, humidity, or gas environment, which are otherwise very challenging. It may thus serve as a versatile high-throughput technique to evaluate single-QD properties and contribute to the development of future generations of QDs with tailored emission properties.

■ METHODS

Synthesis of CdSe/CdS/ZnS Core−Shell−Shell QDs. The batch of CdSe/CdS/ZnS core−shell—shell QDs was the same as in ref 55. The synthesis procedure is described in ref 55.

Synthesis of InP/ZnSe QDs. Nanocrystals were synthesized using a modified method based on Tessier et al.[64] Briefly, a mixture of 100 mg of indium(III) chloride, 300 mg of zinc(II) chloride in 5.0 mL of oleylamine was degassed at 120 °C for 1 h and then heated to 180 °C under nitrogen atmosphere. 0.46 mL of tris-(diethylamino)phosphine was rapidly injected once the mixture reached the temperature of 180 °C. The formation of InP cores proceeded for 20 min, after which 1.08 mL of stoichiometric TOP-Se (1.87 M) was

injected dropwise over the course of 10 min At 140 min, 4 g of zinc stearate dissolved in 4 ml of oleylamine and 16 ml of ODE (both previously degassed) was injected in the reaction mixture. When the temperature reached 180 °C again, 3.36 mL of TOP-Se (1.87 M) was injected dropwise while increasing the temperature to 320 °C. After 240 min the reaction was stopped removing the heat source and cooling with pressurized air. The InP/ZnSe NCs were precipitated by adding 1 eq. volume ethanol and centrifuging at 2750 rpm for 5 min. The precipitate containing the NCs was collected and redispersed in toluene. The washing step with ethanol was repeated twice.

Sample Preparation for Multiparticle Spectroscopy. In MPS, eliminating background luminescence is possibly even more important than in "regular" single-particle spectroscopy, as we use wide-field excitation scheme that may excite fluorescent organic residues and/or impurities in/on the glass coverslip as well as QDs. In the absence of an emission slit, this background light strikes the diffraction grating and subsequently the detector, causing a broad background profile that complicates the identification of single-particle emission spectra. Samples for MPS were prepared by drop-casting 40 μL of QD solution (diluted from the crude QD solution by a factor 10^5–10^7 in spectrophotometric-grade toluene; InP/ZnSe QDs were diluted in a 1 vol % solution of ethyl thioglycolate/toluene) onto glass #1.5 coverslips. After letting the solvent evaporate, the samples were sealed in an inert nitrogen atmosphere. An ideal QD coverage on the glass substrate is around 20−100 particles per $(100 \ \mu m)^2$. To minimize background luminescence, the glass coverslips were cleaned prior to drop-casting the QD solutions, using a low-pressure plasma cleaner (Diener Zepto), operated at 0.2−0.4 mbar, at the maximum power setting.

Multiparticle Spectroscopy. MPS experiments were performed on a homebuilt microscopy setup centered around an inverted microscopy body (Nikon Ti-U) that held the sample. Samples were excited in a wide-field setup using a 445 nm fiber-coupled laser (Coherent OBIS LX, 45 mW), operated at full power in CW mode. The laser light was attenuated using ND filters and focused onto the back-focal plane of an oil-immersion objective (Nikon CFI Plan Apochromat Lambda 100×, NA 1.45), using a dichroic long-pass mirror. A laser beam expander was used so that the excitation spot on the sample surface was approximately Gaussian with a full width at half-maximum (fwhm) of 60 μm. To optimize the luminescence signal while limiting possible effects of photodegradation, we used mild CW excitation powers of 20−80 W/cm^2.

Luminescence was collected using the same objective and was filtered using a 550 nm long-pass and 700 nm short-pass filter for the measurements on CdSe/CdS/ZnS and a 500 nm long-pass and 900 nm short-pass filter for the measurements on InP/ZnSe (Thorlabs FELH550/FESH700 and FELH500/FESH900). The emission light was then directed at the entrance of a spectrometer (Andor Kymera 193i) equipped with a reflective diffraction grating (150 lines/mm, blazed at 500 nm). The diffraction grating and mirrors inside the spectrometer were positioned so that either the 0th-order or 1st-order diffraction image of the grating was directed at an electron-multiplying CCD camera (Andor iXon Ultra 888). For our measurements on InP/ZnSe QDs, the image was cropped at the entrance of the spectrograph to select a narrow horizontal region of ~6.5 μm (50 pixels). We corrected for the

wavelength-dependent detection efficiency of the setup using a broadband calibrated light source (Ocean Optics HL-3Plus-CAL).

Electron Microscopy Characterization. High-resolution high-angle annular dark-field scanning transmission electron microscopy (HAADF-STEM) images and EDX maps were acquired on a Thermo Fisher Scientific/FEI Titan microscope operated at 300 kV. HAADF-STEM images and EDX maps were acquired with a 50 pA and 150 pA current, respectively.

ASSOCIATED CONTENT

Supporting Information

The Supporting Information is available free of charge at https://pubs.acs.org/doi/10.1021/acsphotonics.3c00420.

> Ensemble absorption spectra, further details related to the background-subtraction procedure and spectrum calibration, fitting procedures and fit uncertainties, experimental artifacts, description of the theoretical model of charge diffusion on a QD, and EDX maps of CdSe/CdS/ZnS QDs (PDF)

AUTHOR INFORMATION

Corresponding Author

Freddy T. Rabouw − *Debye Institute for Nanomaterials Science, Utrecht University, 3584CC Utrecht, The Netherlands;* orcid.org/0000-0002-4775-0859; Email: f.t.rabouw@uu.nl

Authors

Mark J. J. Mangnus − *Debye Institute for Nanomaterials Science, Utrecht University, 3584CC Utrecht, The Netherlands;* orcid.org/0000-0002-3595-8097

Jur W. de Wit − *Debye Institute for Nanomaterials Science, Utrecht University, 3584CC Utrecht, The Netherlands*

Sander J. W. Vonk − *Debye Institute for Nanomaterials Science, Utrecht University, 3584CC Utrecht, The Netherlands;* orcid.org/0000-0002-4650-9473

Jaco J. Geuchies − *Optoelectronic Materials Section, Faculty of Applied Sciences, Delft University of Technology, 2629 HZ Delft, The Netherlands*

Wiebke Albrecht − *EMAT, University of Antwerp, 2020 Antwerp, Belgium; NANOlab Center of Excellence, University of Antwerp, 2020 Antwerp, Belgium;* orcid.org/0000-0002-0800-4933

Sara Bals − *EMAT, University of Antwerp, 2020 Antwerp, Belgium; NANOlab Center of Excellence, University of Antwerp, 2020 Antwerp, Belgium;* orcid.org/0000-0002-4249-8017

Arjan J. Houtepen − *Optoelectronic Materials Section, Faculty of Applied Sciences, Delft University of Technology, 2629 HZ Delft, The Netherlands;* orcid.org/0000-0001-8328-443X

Complete contact information is available at:
https://pubs.acs.org/10.1021/acsphotonics.3c00420

Author Contributions

The manuscript was written through contributions of all authors. All authors have given approval to the final version of the manuscript.

ACKNOWLEDGMENTS

REFERENCES

(1) Efros, A. L.; Brus, L. E. Nanocrystal Quantum Dots: From Discovery to Modern Development. *ACS Nano* **2021**, *15*, 6192−6210.

(2) Shirasaki, Y.; Supran, G. J.; Bawendi, M. G.; Bulovic, V. Emergence of Colloidal Quantum-Dot Light-Emitting Technologies. *Nat. Photonics* **2013**, *7*, 13−23.

(3) Liu, Z.; Lin, C.-H.; Hyun, B.-R.; Sher, C.-W.; Lv, Z.; Luo, B.; Jiang, F.; Wu, T.; Ho, C.-H.; Kuo, H.-C.; He, J.-H. Micro-Light-Emitting Diodes with Quantum Dots in Display Technology. *Light Sci. Appl.* **2020**, *9*, No. 83.

(4) Jung, H.; Ahn, N.; Klimov, V. I. Prospects and Challenges of Colloidal Quantum Dot Laser Diodes. *Nat. Photonics* **2021**, *15*, 643−655.

(5) Liu, X.; Braun, G. B.; Zhong, H.; Hall, D. J.; Han, W.; Qin, M.; Zhao, C.; Wang, M.; She, Z.-G.; Cao, C.; Sailor, M. J.; Stallcup, W. B.; Ruoslahti, E.; Sugahara, K. N. Tumor-Targeted Multimodal Optical Imaging with Versatile Cadmium-Free Quantum Dots. *Adv. Funct. Mater.* **2016**, *26*, 267−276.

(6) Kovalenko, M. V. Opportunities and Challenges for Quantum Dot Photovoltaics. *Nat. Nanotechnol.* **2015**, *10*, 994−997.

(7) Qiu, F.; Han, Z.; Peterson, J. J.; Odoi, M. Y.; Sowers, K. L.; Krauss, T. D. Photocatalytic Hydrogen Generation by CdSe/CdS Nanoparticles. *Nano Lett.* **2016**, *16*, 5347−5352.

(8) Meinardi, F.; McDaniel, H.; Carulli, F.; Colombo, A.; Velizhanin, K. A.; Makarov, N. S.; Simonutti, R.; Klimov, V. I.; Brovelli, S. Highly Efficient Large-Area Colourless Luminescent Solar Concentrators Using Heavy-Metal-Free Colloidal Quantum Dots. *Nat. Nanotechnol.* **2015**, *10*, 878−885.

(9) Cohen, T. A.; Milstein, T. J.; Kroupa, D. M.; MacKenzie, J. D.; Luscombe, C. K.; Gamelin, D. R. Quantum-Cutting Yb³⁺-Doped Perovskite Nanocrystals for Monolithic Bilayer Luminescent Solar Concentrators. *J. Mater. Chem. A* **2019**, *7*, 9279−9288.

(10) Protesescu, L.; Yakunin, S.; Bodnarchuk, M. I.; Krieg, F.; Caputo, R.; Hendon, C. H.; Yang, R. X.; Walsh, A.; Kovalenko, M. V. Nanocrystals of Cesium Lead Halide, Perovskites (CsPbX₃, X = Cl, Br, and I): Novel Optoelectronic Materials Showing Bright Emission with Wide Color Gamut. *Nano Lett.* **2015**, *15*, 3692−3696.

(11) Berends, A. C.; Mangnus, M. J. J.; Xia, C.; Rabouw, F. T.; de Mello Donega, C. Optoelectronic Properties of Ternary I−III−VI₂ Semiconductor Nanocrystals: Bright Prospects with Elusive Origins. *J. Phys. Chem. Lett.* **2019**, *10*, 1600−1616.

(12) Ebenstein, Y.; Mokari, T.; Banin, U. Fluorescence Quantum Yield of CdSe/ZnS Nanocrystals Investigated by Correlated Atomic-Force and Single-Particle Fluorescence Microscopy. *Appl. Phys. Lett.* **2002**, *80*, 4033−4305.

(13) Zang, H.; Li, H.; Makarov, N. S.; Velizhanin, K. A.; Wu, K.; Park, Y.-S.; Klimov, V. I. Thick-Shell CuInS₂/ZnS Quantum Dots with Suppressed "Blinking" and Narrow Single-Particle Emission Line Widths. *Nano Lett.* **2017**, *17*, 1787−1795.

(14) Hinterding, S. O. M.; Mangnus, M. J. J.; Prins, P. T.; Jöbsis, H. J.; Busatto, S.; Vanmaekelbergh, D.; de Mello Donega, C.; Rabouw, F. T. Unusual Spectral Diffusion of Single CuInS₂ Quantum Dots Sheds

Light on the Mechanism of Radiative Decay. *Nano Lett.* **2021**, *21*, 658−665.

(15) Nirmal, M.; Dabbousi, B. O.; Bawendi, M. G.; Macklin, J. J.; Trautman, J. L.; Harris, T. D.; Brus, L. E. Fluorescence Intermittency in Single Cadmium Selenide Nanocrystals. *Nature* **1996**, *383*, 802−804.

(16) Blanton, S. A.; Hines, M. A.; Guyot-Sionnest, P. Photoluminescence Wandering in Single CdSe Nanocrystals. *Appl. Phys. Lett.* **1996**, *69*, 3905−3907.

(17) Galland, C.; Ghosh, Y.; Steinbrück, A.; Sykora, M.; Hollingsworth, J. A.; Klimov, V. I.; Htoon, H. Two Types of Luminescence Blinking Revealed by Spectroelectrochemistry of Single Quantum Dots. *Nature* **2011**, *479*, 203−207.

(18) Empedocles, S. A.; Bawendi, M. G. Influence of Spectral Diffusion on the Line Shapes of Single CdSe Nanocrystallite Quantum Dots. *J. Phys. Chem. B* **1999**, *103*, 1826−1830.

(19) Müller, J.; Lupton, J. M.; Rogach, A. L.; Feldmann, J.; Talapin, D. V.; Weller, H. Monitoring Surface Charge Migration in the Spectral Dynamics of Single CdSe/CdS Nanodot/Nanorod Heterostructures. *Phys. Rev. B* **2005**, *72*, No. 205339.

(20) Frantsuzov, P. A.; Marcus, R. A. Explanation of Quantum Dot Blinking Without the Long-Lived Trap Hypothesis. *Phys. Rev. B* **2005**, *72*, No. 155321.

(21) Gómez, D. E.; van Embden, J.; Mulvaney, P. Spectral Diffusion of Single Semiconductor Nanocrystals: The Influence of the Dielectric Environment. *Appl. Phys. Lett.* **2006**, *88*, No. 154106.

(22) Plakhotnik, T.; Fernée, M. J.; Littleton, B.; Rubinsztein-Dunlop, H.; Potzner, C.; Mulvaney, P. Anomalous Power Laws of Spectral Diffusion in Quantum Dots: a Connection to Luminescence Intermittency. *Phys. Rev. Lett.* **2010**, *105*, No. 167402.

(23) Voznyy, O. Mobile Surface Traps in CdSe Nanocrystals with Carboxylic Acid Ligands. *J. Phys. Chem. C* **2011**, *115*, 15927−15932.

(24) Fernée, M. J.; Plakhotnik, T.; Louyer, Y.; Littleton, B. N.; Potzner, C.; Tamarat, P.; Mulvaney, P.; Lounis, B. Spontaneous Spectral Diffusion in CdSe Quantum Dots. *J. Phys. Chem. Lett.* **2012**, *3*, 1716−1720.

(25) Park, K.; Deutsch, Z.; Li, J. J.; Oron, D.; Weiss, S. Single Molecule Quantum-Confined Stark Effect Measurements of Semiconductor Nanoparticles at Room Temperature. *ACS Nano* **2012**, *6*, 10013−10023.

(26) Efros, A. L.; Nesbitt, D. J. Origin and Control of Blinking in Quantum Dots. *Nat. Nanotechnol.* **2016**, *11*, 661−671.

(27) Mahler, B.; Spinicelli, P.; Buil, S.; Quelin, X.; Hermier, J.-P.; Dubertret, B. Towards Non-Blinking Colloidal Quantum Dots. *Nat. Mater.* **2008**, *7*, 659−664.

(28) Chen, O.; Zhao, J.; Chauhan, V. P.; Cui, J.; Wong, C.; Harris, D. K.; Wei, H.; Han, H.-S.; Fukumura, D.; Jain, R. K.; Bawendi, M. G. Compact High-Quality CdSe-CdS Core-Shell Nanocrystals with Narrow Emission Linewidths and Suppressed Blinking. *Nat. Mater.* **2013**, *12*, 445−451.

(29) Park, Y.-S.; Lim, J.; Klimov, V. I. Asymmetrically Strained Quantum Dots with Non-Fluctuating Single-Dot Emission Spectra and Subthermal Room-Temperature Linewidths. *Nat. Mater.* **2019**, *18*, 249−255.

(30) Reid, K. R.; McBride, J. R.; Freymeyer, N. J.; Thal, L. B.; Rosenthal, S. J. Chemical Structure, Ensemble and Single-Particle Spectroscopy of Thick-Shell InP−ZnSe Quantum Dots. *Nano Lett.* **2018**, *18*, 709−716.

(31) Chandrasekaran, V.; Tessier, M. D.; Dupont, D.; Geiregat, P.; Hens, Z.; Brainis, E. Nearly Blinking-Free, High-Purity Single-Photon Emission by Colloidal InP/ZnSe Quantum Dots. *Nano Lett.* **2017**, *17*, 6104−6109.

(32) Kim, T.; Won, Y.-H.; Jang, E.; Kim, D. Negative Trion Auger Recombination in Highly Luminescent InP/ZnSe/ZnS Quantum Dots. *Nano Lett.* **2021**, *21*, 2111−2116.

(33) Lee, Y.; Jo, D.-Y.; Kim, T.; Jo, J.-H.; Park, J.; Yang, H.; Kim, D. Effectual Interface and Defect Engineering for Auger Recombination Suppression in Bright InP/ZnSeS/ZnS Quantum Dots. *ACS Appl. Mater. Interfaces* **2022**, *14*, 12479−12487.

(34) Won, Y.-H.; Cho, O.; Kim, T.; Chung, D.-Y.; Kim, T.; Chung, H.; Jang, H.; Lee, J.; Kim, D.; Jang, E. Highly Efficient and Stable InP/ZnSe/ZnS Quantum Dot Light-Emitting Diodes. *Nature* **2019**, *575*, 634−638.

(35) Van Avermaet, H.; Schiettecatte, P.; Hinz, S.; Giordano, L.; Ferrati, F.; Nayral, C.; Delpech, F.; Maultzsch, J.; Lange, H.; Hens, Z. Full-Spectrum InP-Based Quantum Dots with Near-Unity Photoluminescence Quantum Efficiency. *ACS Nano* **2022**, *16*, 9701−9712.

(36) Sousa Velosa, F.; van Avermaet, H.; Schiettecatte, P.; Mingabudinova, L.; Geiregat, P.; Hens, Z. State Filling and Stimulated Emission by Colloidal InP/ZnSe Core/Shell Quantum Dots. *Adv. Opt. Mater.* **2022**, *10*, No. 2200328.

(37) Berkinsky, D. B.; Proppe, A. H.; Utzat, H.; Krajewska, C. J.; Sun, W.; Sverko, T.; Yoo, J. J.; Chung, H.; Won, Y.-H.; Kim, T.; Jang, E.; Bawendi, M. G. Narrow Intrinsic Line Widths and Electron−Phonon Coupling of InP Quantum Dots. *ACS Nano* **2023**, *17*, 3598−3609.

(38) Jeong, B. G.; Chang, J. H.; Hahm, D.; Rhee, S.; Park, M.; Lee, S.; Kim, Y.; Shin, D.; Park, J. W.; Lee, C.; Lee, D. C.; Park, K.; Hwang, E.; Bae, W. K. Interface Polarization in Heterovalent Core−Shell Nanocrystals. *Nat. Mater.* **2022**, *21*, 246−252.

(39) Janke, E. M.; Williams, N. E.; She, C.; Zherebetskyy, D.; Hudson, M. H.; Wang, L.; Gosztola, D. J.; Schaller, R. D.; Lee, B.; Sun, C.; Engel, G. S.; Talapin, D. V. Origin of Broad Emission Spectra in InP Quantum Dots: Contributions from Structural and Electronic Disorder. *J. Am. Chem. Soc.* **2018**, *140*, 15791−15803.

(40) Hughes, K. E.; Stein, J. L.; Friedfeld, M. R.; Cossairt, B. M.; Gamelin, D. R. Effects of Surface Chemistry on the Photophysics of Colloidal InP Nanocrystals. *ACS Nano* **2019**, *13*, 14198−14207.

(41) Nguyen, A. T.; Jen-La Plante, I.; Ippen, C.; Ma, R.; Kelley, D. F. Extremely Slow Trap-Mediated Hole Relaxation in Room-Temperature InP/ZnSe/ZnS Quantum Dots. *J. Phys. Chem. C* **2021**, *125*, 4110−4118.

(42) Kelley, A. M.; Cavanaugh, P.; Sun, H.; Wang, X.; Bautista, M. J.; Jen-La Plante, I.; Ippen, C.; Kelley, D. F. Identity of the Reversible Hole Traps in InP/ZnSe Core/Shell Quantum Dots. *J. Chem. Phys.* **2022**, *157*, No. 174701.

(43) Cui, J.; Beyler, A. P.; Marshall, L. F.; Chen, O.; Harris, D. K.; Wanger, D. D.; Brokmann, X.; Bawendi, M. G. Direct Probe of Spectral Inhomogeneity Reveals Synthetic Tunability of Single-Nanocrystal Linewidths. *Nat. Chem.* **2013**, *5*, 602−606.

(44) Beyler, A. P.; Bischof, T. S.; Cui, J.; Coropceanu, I.; Harris, D. K.; Bawendi, M. G. Sample-Averaged Biexciton Quantum Yield Measured by Solution-Phase Photon Correlation. *Nano Lett.* **2014**, *14*, 6792−6798.

(45) Marchioro, A.; Whitham, P. J.; Knowles, K. E.; Kilburn, T. B.; Reid, P. J.; Gamelin, D. R. Tunneling in the Delayed Luminescence of Colloidal CdSe, Cu⁺-Doped CdSe, and CuInS₂ Semiconductor Nanocrystals and Relationship to Blinking. *J. Phys. Chem. C* **2016**, *120*, 27040−27049.

(46) Utzat, H.; Schulenberger, K. E.; Achorn, O. B.; Nasilowski, M.; Sinclair, T. S.; Bawendi, M. G. Probing Linewidths and Biexciton Quantum Yields of Single Cesium Lead Halide Nanocrystals in Solution. *Nano Lett.* **2017**, *17*, 6838−6846.

(47) Empedocles, S. A.; Bawendi, M. G. Quantum-Confined Stark Effect in Single CdSe Nanocrystallite Quantum Dots. *Science* **1997**, *278*, 2114−2117.

(48) Empedocles, S. A.; Norris, D. J.; Bawendi, M. G. Photoluminescence Spectroscopy of Single CdSe Nanocrystallite Quantum Dots. *Phys. Rev. Lett.* **1996**, *77*, 3873.

(49) Houel, J.; Doan, Q. T.; Cajgfinger, T.; Ledoux, G.; Amans, D.; Aubret, A.; Dominjon, A.; Ferriol, S.; Barbier, R.; Nasilowski, M.; Lhuiller, E.; Dubertret, B.; Dujardin, C.; Kulzer, F. Autocorrelation Analysis for the Unbiased Determination of Power-Law Exponents in Single-Quantum-Dot Blinking. *ACS Nano* **2015**, *9*, 886−893.

(50) Howell, S. B. *Handbook of CCD Astronomy*, 2nd ed.; Cambridge University Press, 2006; pp 157−165.

(51) Zhang, Z.; Kenny, S.; Hauser, M.; Li, W.; Xu, K. Ultrahigh-Throughput Single-Molecule Spectroscopy and Spectrally Resolved Super-Resolution Microscopy. *Nat. Methods* **2015**, *12*, 935−938.

(52) Martens, K. J. A.; Gobes, M.; Archontakis, E.; Brillas, R. R.; Zijlstra, N.; Albertazzi, L.; Hohlbein, J. Enabling Spectrally Resolved Single-Molecule Localization at High Emitter Densities. *Nano Lett.* **2022**, *22*, 8618−8625.

(53) Brokmann, X.; Bawendi, M. G.; Coolen, L.; Hermier, J.-P. Photon-Correlation Spectroscopy. *Opt. Express* **2006**, *14*, 6333−6341.

(54) Marshall, L. F.; Cui, J.; Brokmann, X.; Bawendi, M. G. Extracting Spectral Dynamics from Single Chromophores in Solution. *Phys. Rev. Lett.* **2010**, *105*, No. 053005.

(55) Vonk, S. J. W.; Heemskerk, B. A. J.; Keiter, R. C.; Hinterding, S. O. M.; Geuchies, J. J.; Houtepen, A. J.; Rabouw, F. T. Biexciton Binding Energy and Line Width of Single Quantum Dots at Room Temperature. *Nano Lett.* **2021**, *21*, 5760−5766.

(56) Brodu, A.; Ballottin, M. V.; Buhot, J.; van Harten, E. J.; Dupont, D.; La Porta, A.; Prins, P. T.; Tessier, M. D.; Versteegh, M. A. M.; Zwiller, V.; Bals, S.; Hens, Z.; Rabouw, F. T.; Christianen, P. C. M.; de Mello Donega, C.; Vanmaekelbergh, D. Exciton Fine Structure and Lattice Dynamics in InP/ZnSe Core/Shell Quantum Dots. *ACS Photonics* **2018**, *5*, 3353−3362.

(57) Beyler, A. P.; Marshall, L. F.; Cui, J.; Brokmann, X.; Bawendi, M. G. Direct Observation of Rapid Discrete Spectral Dynamics in Single Colloidal CdSe-CdS Core-Shell Quantum Dots. *Phys. Rev. Lett.* **2013**, *111*, No. 177401.

(58) Neuhauser, R. G.; Shimizu, K. T.; Woo, W. K.; Empedocles, S. A.; Bawendi, M. G. Correlation between Fluorescence Intermittency and Spectral Diffusion in Single Semiconductor Quantum Dots. *Phys. Rev. Lett.* **2000**, *85*, 3301.

(59) Ihara, T.; Kanemitsu, Y. Spectral Diffusion of Neutral and Charged Exciton Transitions in Single CdSe/ZnS Nanocrystals due to Quantum-Confined Stark Effect. *Phys. Rev. B* **2014**, *90*, No. 195302.

(60) Ekimov, A. I.; Hache, F.; Schanne-Klein, M. C.; Ricard, D.; Flytzanis, C.; Kudryavtsev, I. A.; Yazeva, T. V.; Rodina, A. V.; Efros, Al. L. Absorption and Intensity-Dependent Photoluminescence Measurements on CdSe Quantum Dots: Assignment of the First Electronic Transitions. *J. Opt. Soc. Am. B* **1993**, *10*, 100−107.

(61) Norris, D. J.; Bawendi, M. G. Measurement and Assignment of the Size-Dependent Optical Spectrum in CdSe Quantum Dots. *Phys. Rev. B* **1996**, *53*, 16338.

(62) Brichkin, S. B.; Spirin, M. G.; Tovstun, S. A.; Gak, V. Y.; Mart'yanova, E. G.; Razumov, V. F. Colloidal Quantum Dots InP@ZnS: Inhomogeneous Broadening and Distribution of Luminescence Lifetimes. *High Energy Chem* **2016**, *50*, 395−399.

(63) De, C. K.; Routh, T.; Roy, D.; Mandal, S.; Mandal, P. K. Highly Photoluminescent InP Based Core Alloy Shell QDs from Air-Stable Precursors: Excitation Wavelength Dependent Photoluminescence Quantum Yield, Photoluminescence Decay Dynamics, and Single Particle Blinking Dynamics. *J. Phys. Chem. C* **2018**, *122*, 964−973.

(64) Tessier, M. D.; Dupont, D.; De Nolf, K.; De Roo, J.; Hens, Z. Economic and Size-Tunable Synthesis of InP/ZnE (E = S, Se) Colloidal Quantum Dots. *Chem. Mater.* **2015**, *27*, 4893−4898.

(65) Loiudice, A.; Lecina, O. S.; Bornet, A.; Luther, J. M.; Buonsanti, R. Ligand Locking on Quantum Dot Surfaces via a Mild Reactive Surface Treatment. *J. Am. Chem. Soc.* **2021**, *143*, 13418−13427.

(66) Tamarat, P.; Bodnarchuk, M. I.; Trebbia, J.-B.; Erni, R.; Kovalenko, M. V.; Even, J.; Lounis, B. The Ground Exciton State of Formamidinium Lead Bromide Perovskite Nanocrystals is a Singlet Dark State. *Nat. Mater.* **2019**, *18*, 717−724.

(67) Chen, X.; Nazzal, A.; Goorskey, D.; Xiao, M.; Peng, Z. A.; Peng, X. Polarization Spectroscopy of Single CdSe Quatum Rods. *Phys. Rev. B* **2001**, *64*, No. 245304.